Burns & Trauma, 2022, 10, tkac010
https://doi.org/10.1093/burnst/tkac010
Research Article

OXFORD

Research Article

Nerve transfer with 3D-printed branch nerve conduits

Jing Zhang[1,†], Jie Tao[2,3,†], Hao Cheng[2,†], Haofan Liu[2], Wenbi Wu[2], Yinchu Dong[2], Xuesong Liu[1], Maling Gou[2], Siming Yang[4,*] and Jianguo Xu[1,*]

[1]Department of Neurosurgery, National Clinical Research Center for Geriatrics, West China Hospital, Sichuan University, Chengdu 610041, P. R. China, [2]State Key Laboratory of Biotherapy and Cancer Center, West China Hospital, Sichuan University, Chengdu 610041, P. R. China, [3]Department of Stomatology, Daping Hospital, Third Military Medical University, Chongqing 400042, P. R. China and [4]Key Laboratory of Wound Repair and Regeneration of PLA, Chinese PLA General Hospital, Medical College of PLA, Beijing 100853, P.R. China

*Correspondence. Jianguo Xu, Email: xujg@scu.edu.cn; Siming Yang, Email: ysm0117@126.com

[†]These authors contributed equally to this work.

Received 16 October 2021; Revised 15 February 2022; Accepted 27 February 2022

Abstract

Background: Nerve transfer is an important clinical surgical procedure for nerve repair by the coaptation of a healthy donor nerve to an injured nerve. Usually, nerve transfer is performed in an end-to-end manner, which will lead to functional loss of the donor nerve. In this study, we aimed to evaluate the efficacy of 3D-printed branch nerve conduits in nerve transfer.
Methods: Customized branch conduits were constructed using gelatine-methacryloyl by 3D printing. The nerve conduits were characterized both *in vitro* and *in vivo*. The efficacy of 3D-printed branch nerve conduits in nerve transfer was evaluated in rats through electrophysiology testing and histological evaluation.
Results: The results obtained showed that a single nerve stump could form a complex nerve network in the 3D-printed multibranch conduit. A two-branch conduit was 3D printed for transferring the tibial nerve to the peroneal nerve in rats. In this process, the two branches were connected to the distal tibial nerve and peroneal nerve. It was found that the two nerves were successfully repaired with functional recovery.
Conclusions: It is implied that the two-branch conduit could not only repair the peroneal nerve but also preserve partial function of the donor tibial nerve. This work demonstrated that 3D-printed branch nerve conduits provide a potential method for nerve transfer.

Key words: Branch nerve conduit, Nerve transfer, 3D printing, Nerve regeneration

Highlights

- In this study, a customized branch nerve conduit for nerve transfer was constructed by 3D printing.
- It was demonstrated that a single nerve stump could form a complex nerve network in the 3D-printed multibranch conduit.
- In rat models, the two-branch nerve conduit could not only repair the injured peroneal nerve but also preserve partial function of the donor tibial nerve, demonstrating the potential utility of 3D-printed branch nerve conduits in nerve transfer.

Background

Peripheral nerve injury occurs in ~2–5% of all trauma patients [1,2] and often leads to functional impairment and significant deterioration in quality of life [3,4]. Primary end-to-end anastomosis of the nerve stumps shows the best results and is preferred [5,6]. When the proximal stump of the nerve is not available for anastomosis, nerve transfer to the distal stump using another nerve is the favored surgical procedure [5]. For example, in patients with lesions involving the temporal bone or cerebellopontine angle, the proximal stump of the facial nerve may be injured and nerve transfer by another nerve is the favored surgical technique to repair the facial nerve [7]. Masseteric-facial nerve anastomosis is one of the surgical procedures for early facial reanimation [8]. Biglioli *et al*. performed masseteric-facial nerve anastomosis with an interposition nerve graft of the great auricular nerve and showed good facial nerve recovery [8]. However, complete transection of the masseteric nerve and end-to-end nerve transfer would inevitably sacrifice the normal function of the masseteric nerve. Alternative side-to-end nerve transfer could overcome this shortcoming. Hypoglossal-facial nerve anastomosis is also a popular and effective surgical technique. Manni *et al*. performed indirect hypoglossal-facial nerve anastomosis with a free greater auricular nerve end-to-side to the hypoglossal nerve and end-to-end to the distal facial nerve and suggested the use of this technique to preserve partial function of the hypoglossal nerve [5]. However, this type of side-to-end surgery is slightly inconvenient to perform. Similar conditions also occur in the surgeries of brachial plexus avulsion injuries and other cases [9,10]. To overcome the limitations of sacrificing healthy nerves in end-to-end surgery and the inconvenience of side-to-end surgery, novel strategies are needed. One potential strategy may be the use of branch nerve conduits, by which the donor nerve could both repair the injured nerve and preserve its own function.

3D printing, which allows for customized manufacturing, has been increasingly employed in the biomedical engineering field, such as in tissue engineering and regenerative medicine [11–13]. In this study, digital light processing (DLP)-based 3D printing and gelatine-methacryloyl (GelMA) hydrogels were used for fabrication of branch nerve conduits. Using DLP-based 3D printing technology, we could continuously fabricate customized nerve conduits with rapid speed and high precision compared to conventional 3D printing technologies [14,15]. In our previous studies, nerve conduits made by GelMA hydrogels were found to have favorable mechanical properties and biocompatibility [15,16].

In this study, we first demonstrated that a single nerve stump could form a complex branch nerve network in a multibranch nerve conduit. Then, taking advantage of DLP-based 3D printing technology, we constructed a 3D-printed two-branch nerve conduit (Figure 1). The efficacy of the two-branch nerve conduit was assessed by the transfer of the tibial nerve to the peroneal nerve in rats. Functional and histological evaluation results showed that the two-branch nerve conduit could not only promote the regeneration and functional recovery of the injured peroneal nerve but also preserve the function of the donor nerve, demonstrating the potential utility of this conduit in nerve transfer.

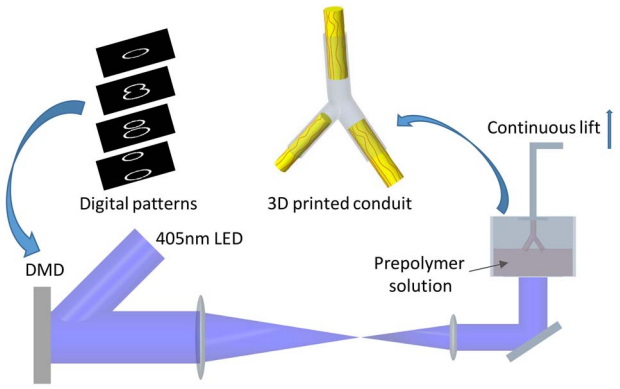

Figure 1. Schematic illustration of the fabrication of customizable 3D-printed two-branch nerve conduits by a rapid continuous 3D printing system. *DMD* digital micromirror device, *LED* light emitting diode

Methods

Materials

The materials used included vitamin B12 (Aladdin, China), Cell Counting Kit-8 (CCK-8, MedChemExpress, USA), Live/Dead Cell Imaging Kit (Life Technologies, USA) and Dulbecco's modified Eagle's medium (DMEM, Invitrogen Co., USA). GelMA and lithium phenyl-2,4,6-trimethylbenzoylphosphinate (LAP) were synthesized as described in previous studies [17,18].

Sprague–Dawley (SD) rats were purchased from the Laboratory Animal Center of Sichuan University (Chengdu, China) and maintained under specific pathogen-free conditions. Rats were acclimatized in the new environment for at least 7 days before any experiments. All animal experimental procedures were approved by the Institutional Animal Care and Use Committee of West China Hospital of Sichuan University and conformed to the guidelines and regulations of Sichuan University Committee on Animal Research and Ethics.

Cell culture

PC12 cells were purchased from ATCC (American Tissue Culture Collection, USA) and cultured at 37°C in a humidified atmosphere containing 5% CO_2. The culture medium was DMEM with 10% (v/v) fetal bovine serum, 100 units/ml penicillin and 100 mg/mL streptomycin (Thermo Scientific, Logan, USA).

Fabrication process of 3D-printed nerve conduits

A DLP-based bioprinter was used to fabricate the nerve conduits [19]. The 2D images of the nerve conduit were uploaded to the digital micromirror device (DMD) chip to generate ultraviolet light patterns. By moving the *z*-axis translation stage, 3D structures were continuously generated. The

printing materials were GelMA (20% w/v), vitamin B12 (0.15% w/v) and LAP (0.7% w/v). Vitamin B12, a photoabsorber, was added to absorb the extra light and improve the printing fidelity. This solution was added to the building platform and polymerized via exposure to 405 nm visible light. It took ∼1 min to print a 1 cm-long conduit. The longer the exposure time to 405 nm light, the higher the degree of crosslinking of the materials and the better the mechanical stability of the conduit. To remove LAP, vitamin B12 and unreacted polymers, the 3D-printed nerve conduits were incubated in phosphate buffered saline (PBS) for 24 h at 37°C.

Characterizations of the nerve conduits

Scanning electron microscopy (SEM, S-4800, Hitachi, Japan) was used to characterize the microstructure of the nerve conduits. The nerve conduits were prepared by gradual dehydration in ethanol solution (15, 30, 45, 60, 75, 95 and 100%). After critical-point drying and Pt/C shadowing, the samples were evaluated using SEM.

The 3D-printed nerve conduits were observed under a light microscope to characterize the surface microstructure of GelMA.

Cell viability was assessed using a live/dead cell kit to evaluate the biocompatibility of the 3D-printed nerve conduits. The printing solution (300 μL) was polymerized in a 24-well plate via exposure to 405 nm visible light and incubated in PBS for 24 h at 37°C to remove the photoinitiator and unreacted polymers. Then, PC12 cells were seeded on the hydrogel in a 24-well plate. Then, 1 μL of the propidium iodide (PI) solution was added to 2 mL of the PBS solution. Then, 1 μL of the Calcein AM solution was added to prepare 8 μM PI and 2 μM Calcein AM mixed liquids. A total of 500 μL of mixed liquid was added to each well of a 24-well plate in which PC12 cells were cocultured with the above-mentioned hydrogel. After incubating for 30 min, the working solution in each well was removed. Then, 1 mL of the PBS solution was added to each well and the cells were observed under a fluorescence microscope.

A CCK-8 assay was also performed *in vitro*. PC12 cells were seeded on the above-mentioned hydrogel in a 24-well plate. At the predesigned time points (24, 48 and 72 h), 30 μL of the CCK-8 reagent was added to each well and incubated for 2 h. The supernatant liquid was transferred to a 96-well plate and the absorbance was measured at 450 nm using a microplate reader.

The mechanical properties of the nerve conduit were assessed by a dynamic mechanical analyzer (DMA, Q800 TA Instruments). The controlled force mode was applied to evaluate the compression mechanical properties of the nerve conduit. The assessment was performed at 25°C.

To investigate the biocompatibility *in vivo*, 3D-printed nerve conduits were implanted subcutaneously on the backs of SD rats. The implanted sites were exposed at different time points (4, 8 and 12 weeks). The nerve conduits and surrounding tissues were harvested and fixed in 4% paraformaldehyde for histological examination. The harvested samples were embedded in paraffin and 5 μm paraffin sections were prepared. Hematoxylin and eosin (H&E) staining was performed and sections were observed under a light microscope.

Surgical process

Adult male SD rats (200–220 g) were used in this study. Animals were anesthetized by intraperitoneal injection of chloral hydrate (0.3 mL/100 g). After anaesthetization, the hair on the right leg was shaved. After disinfection and surgical field draping, a skin incision of ∼3 cm was made. Then, the sciatic nerve and its branches were exposed. To implant the 3D-printed multibranch nerve conduit, complete tibial nerve transection was performed. The 3D-printed multibranch nerve conduit was then immediately implanted, with the upper part sutured with the tibial nerve and the lower part embedded in the adjacent muscle.

To evaluate the efficacy of the two-branch nerve conduit, rats (200–220 g) were randomly divided into three groups of six animals each: end-to-end autograft group, side-to-end autograft group and 3D-printed two-branch nerve conduit group (branch group). For animals in the end-to-end group, both the tibial nerve and peroneal nerve were cut off and 10 mm of the distal peroneal nerve was surgically removed. Then, the proximal stump of the tibial nerve and the distal stump of the peroneal nerve were bridged with the transected peroneal nerve using 8–0 absorbable Vicryl sutures. For animals in the side-to-end group, 10 mm of the peroneal nerve was also surgically removed and a 5 mm branch of the tibial nerve was carefully made. Then, the branch of the tibial nerve and the distal stump of the peroneal nerve were bridged with the transected peroneal nerve. For animals in the branch group, 10 mm of both the tibial nerve and peroneal nerve were surgically removed. Then, the proximal stump of the tibial nerve and the two stumps of the distal tibial nerve and peroneal nerve were bridged with the 3D-printed two-branch nerve conduit. Then, the muscle and skin layers were sutured with 2–0 nylon sutures.

Electrophysiology

Functional evaluation of the peroneal nerves (all three groups) and tibial nerve (side-to-end group and branch group) 3 months after surgery was carried out by electrophysiology testing. Briefly, animals were anesthetized by intraperitoneal injection of chloral hydrate (0.3 mL/100 g) before electrophysiological evaluation. After the peroneal and tibial nerves were exposed, bipolar stimulating electrodes were placed on the proximal and distal parts of the regenerated nerve. The monopolar recording electrode was placed in the tibial anterior for peroneal nerve evaluation and gastrocnemius for tibial nerve evaluation. The nerve conduction velocity (NCV), latency of compound muscle action potential (CMAP)

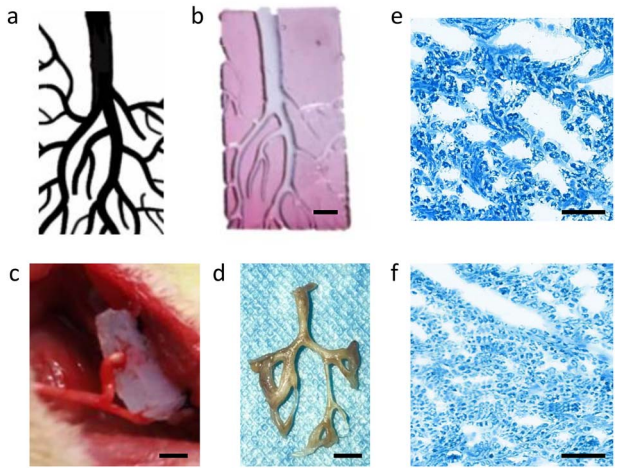

Figure 2. Complex nerve network formed by a single nerve stump in a multibranch nerve conduit. (**a**) Digital patterns of the multibranch nerve conduit. (**b**) 3D-printed multibranch nerve conduit (scale bar: 0.2 cm). (**c**) The 3D-printed multibranch nerve conduit was implanted in rats, with the upper part sutured with the tibial nerve and the lower part embedded in the adjacent muscle; scale bar = 0.2 cm. (**d**) Successful reconstruction of the complicated nerve network in the multibranch nerve conduit, scale bar = 0.25 cm. Representative Luxol fast blue staining images of the regenerated main nerve (**e**) and branch nerve (**f**) (scale bar = 50 μm)

onset and peak amplitude of CMAP were measured by an electromyography machine (Nuocheng, Shanghai, China).

Histological evaluation

After electrophysiological testing, the peroneal nerve, tibial nerve, tibial anterior and gastrocnemius from each group were harvested, weighed (muscles) and then fixed in 10% formalin for >24 h. The tissues were embedded in paraffin after gradient dehydration and 5 μm paraffin sections were prepared. H&E staining and Luxol fast blue (LFB) staining were performed and sections were observed under a light microscope.

To further evaluate the axons and myelin sheath of the regenerated peroneal nerve and tibial nerve, the distal parts of the regenerated nerve specimens were cut and fixed in 2.5% glutaraldehyde solution. Then, the nerves were fixed with 1% osmium tetroxide solution for 2 h followed by washing and gradient dehydration. Ultrathin sections (thickness, 80 nm) were prepared and stained with lead citrate and uranyl acetate. The sections were observed by transmission electron microscopy (TEM) (HT7700; Hitachi). The diameters of the axons and thickness of the myelin sheath were evaluated by ImageJ software.

Statistical analysis

The Shapiro–Wilk normality test was used for normality distribution analysis. The unpaired t-test was used for analysis of two groups. For analysis of three groups, Tukey's multiple comparisons test, with a single pooled variance, was used to correct for multiple comparisons using statistical hypothesis testing. Each p value was adjusted to account for multiple comparisons. All statistical analyses were conducted by GraphPad Prism 5 (GraphPad Software Inc., USA). The experimental data are expressed as the means with standard deviations, and $p < 0.05$ was considered statistically significant.

Results

A single nerve stump forms a complex nerve network in a multibranch conduit

First, we aimed to determine whether a single nerve stump could extend to form a multibranch nerve network. A multibranch nerve conduit was designed (Figure 2a) and 3D-printed (Figure 2b) by the previously established DLP-based rapid continuous 3D printing platform. In the upper part, we designed a straight hollow sleeve so that the proximal end of the cut nerve could be inserted and sutured to the sleeve. In the lower part, we designed a tree-like network for the reconstruction of the complex nerve branch.

Then, the 3D-printed multibranch nerve conduit was implanted in the rat, as described above (Figure 2c). One month after implantation, the regenerated nerve network was harvested (Figure 2d) and paraffin sections were prepared for histological evaluation. The regenerated tibial nerve was split into two main branches and then split further into tree-like nerve networks. LFB staining was performed on sections at different locations of the nerve network. Representative LFB staining images of the regenerated main nerve and branch nerve are shown in Figure 2e and f, respectively, and axons were found across the entire nerve network. The above-mentioned results demonstrated that one single nerve stump could form a complex branch nerve network through the guidance of the multibranch conduit.

Fabrication and characterization of 3D-printed two-branch nerve conduits

Next, we prepared a two-branch nerve conduit to evaluate its effect on nerve transfer. Through DLP-based 3D printing, the two-branch nerve conduit could be successfully prepared within 2 min. A photograph of the two-branch nerve conduit is shown in Figure 3a. The main conduit and the two branches were all 5 mm in length, 1 mm in inner diameter and 2 mm in outer diameter. The angle between the two branches was 36°. The micromorphology of the nerve conduit was observed by SEM (Figure 3b). The surface structure of the 3D-printed nerve conduit was also observed under a light microscope. As shown in Figure 3c, the nerve conduit had a directional and continuous microstructure. Previous studies have demonstrated that the surface structure of the nerve conduit could affect the growth of cells [20] and that longitudinal surface topography could facilitate oriented cell migration and neurite extension during nerve regeneration [21]. Continuous microstructure could improve the structural integrity and mechanical properties of the nerve conduit

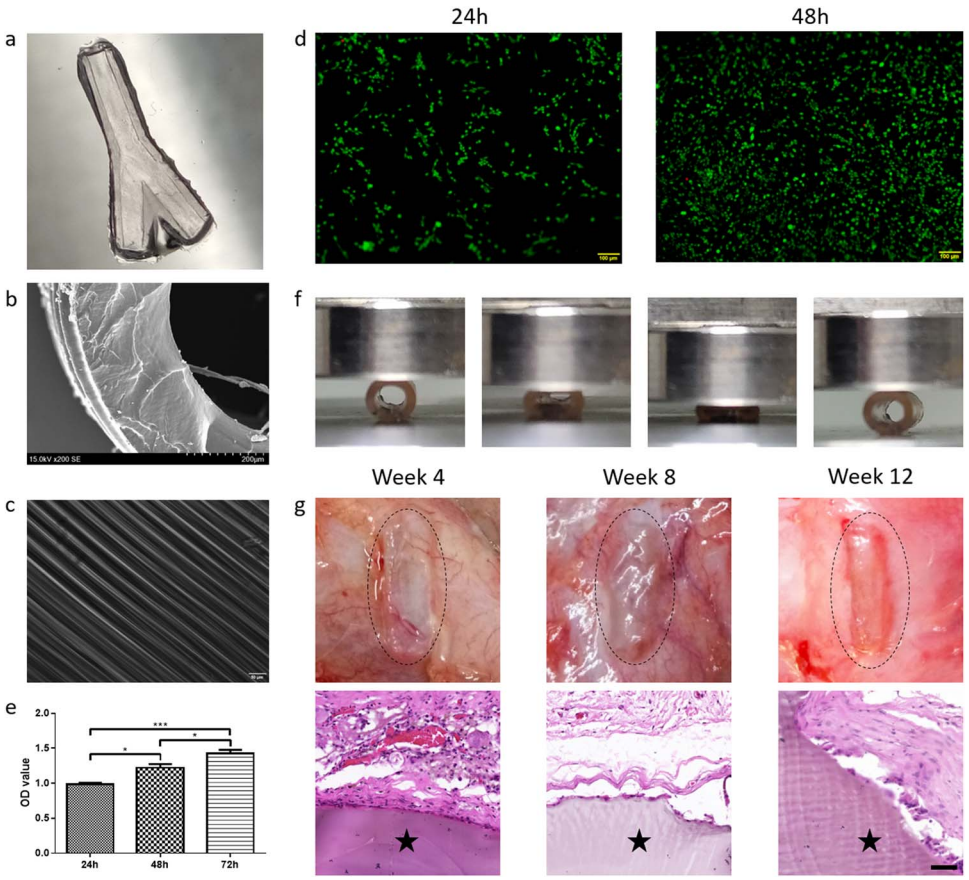

Figure 3. Preparation and characterization of the 3D-printed two-branch nerve conduit. (**a**) Photograph of the 3D-printed two-branch nerve conduit. (**b**) Scanning electron microscopy image of the nerve conduit (scale bar = 100 μm). (**c**) Surface microstructure of the nerve conduit. (**d**) The live/dead cell imaging kit detects the survival and proliferation of the PC12 cells on GelMA hydrogel at 24 and 48 h. (**e**) Quantitative proliferation analysis of PC12 cells by CCK-8 assay. Data are presented as the mean ± standard deviation, $^{*}p < 0.05$, $^{***}p < 0.001$. (**f**) Compression mechanical properties of the nerve conduit. (**g**) Representative images of observation (upper) and hematoxylin and eosin staining (lower) of the conduits at 4, 8 and 12 weeks following subcutaneous implantation in rats (star: conduit; scale bar = 50 μm)

[14,16]. Therefore, printed nerve conduits with directional and continuous microstructures have good potential to facilitate peripheral nerve regeneration.

To evaluate the cytocompatibility of the hydrogel conduits, a live/dead cell kit and CCK-8 assay were utilized for PC12 cell viability and proliferation analysis. The fluorescent images of live/dead-stained PC12 cells adhered to the hydrogel at 24 and 48 h are shown in Figure 3d. A high percentage of green-colored live cells and few red-colored dead cells were found within 48 h, indicating good cell compatibility of the hydrogel conduits. The CCK-8 assay results suggested that PC12 cells showed a favorable capability for proliferation when cultured on the hydrogel over time (Figure 3e).

The DMA test showed that the nerve conduit was highly elastic. As shown in Figure 3f, after the force was removed the nerve conduit was able to regain its original shape, demonstrating favorable compression mechanical properties of the nerve conduit, thus supporting nerve regeneration.

The *in vivo* biocompatibility of 3D-printed straight nerve conduits was investigated subcutaneously on the backs of SD rats. At different time points (4, 8 and 12 weeks), the embedded conduits were exposed, and they retained their structures at 12 weeks (Figure 3g, upper part). The results obtained suggested that the structures of the conduits were stable in the first 3 months, which allowed stable and favorable guidance for axon extension. As shown in Figure 3g (lower part), there were few inflammatory cells around the hydrogel conduits. Histological examination demonstrated that the embedded conduits did not cause serious inflammation and had good biocompatibility. Taken together, our hydrogel conduits showed a favorable surface microstructure, good compression mechanical properties and good biocompatibility both *in vitro* and *in vivo*, suggesting favorable guidance potential in nerve regeneration.

Functional and histological evaluation *in vivo*

To evaluate the efficacy of our 3D-printed two-branch nerve conduits in nerve transfer *in vivo*, we used the conduits to bridge the proximal stump of the tibial nerve and the two distal stumps of the tibial nerve and peroneal nerve, and autografts were used as controls. SD rats were randomly divided into three groups: end-to-end autograft group, side-to-end

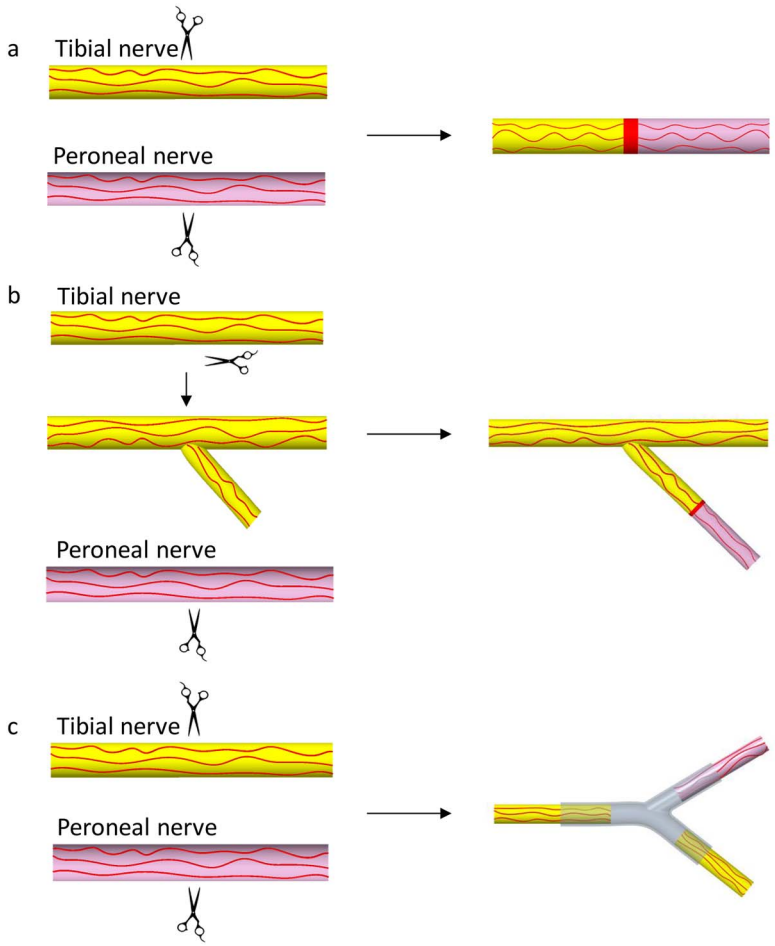

Figure 4. Schematic illustration of the surgical processes. (**a**) End-to-end autograft group, (**b**) side-to-end autograft group and (**c**) branch group

autograft group and branch group. A schematic illustration of the surgical processes is shown in Figure 4.

After the nerve defect models were established, nerve grafts or 3D-printed two-branch nerve conduits were used to bridge the gaps between the proximal stump and distal stump of the nerves in each group (Figure 5a). Three months after the operation, the surgical sites were exposed (Figure 5b) and the regenerated nerves were harvested (Figure 5c). We found that the proximal and distal stumps were all successfully reconnected in the three groups. In the branch group, the tibial nerve split into two branches and reconnected with the distal tibial nerve and peroneal nerve along the 3D-printed branch nerve conduits, showing that our branch nerve conduits could not only repair the injured nerve but also preserve the donor nerve. Meanwhile, in accordance with the degradation study *in vivo*, we found that the implanted nerve conduits were neither degraded nor collapsed, demonstrating that the nerve conduits have favorable mechanical properties, which allows stable guidance for nerve extension. In addition, no neuromas were observed in the surgical sites.

To evaluate the functional recovery of regenerated peroneal nerves, electrophysiological examinations were performed 3 months after surgery. As shown in Figure 6a, the NCV in the end-to-end group (33.3 m/s) was significantly

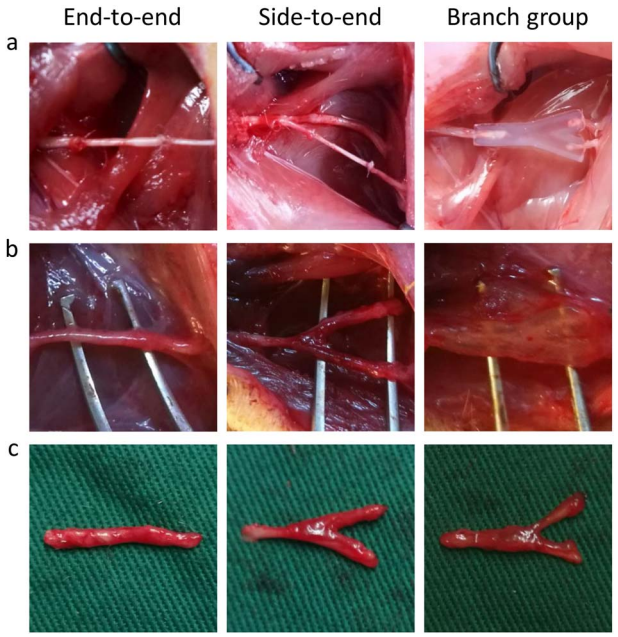

Figure 5. Surgical process and postoperative nerve regeneration. (**a**) Nerve repair surgeries in three different groups. (**b**) The regenerated nerves were surgically exposed after 3 months in three different groups. (**c**) Representative photographs of regenerated nerves in different groups after 3 months

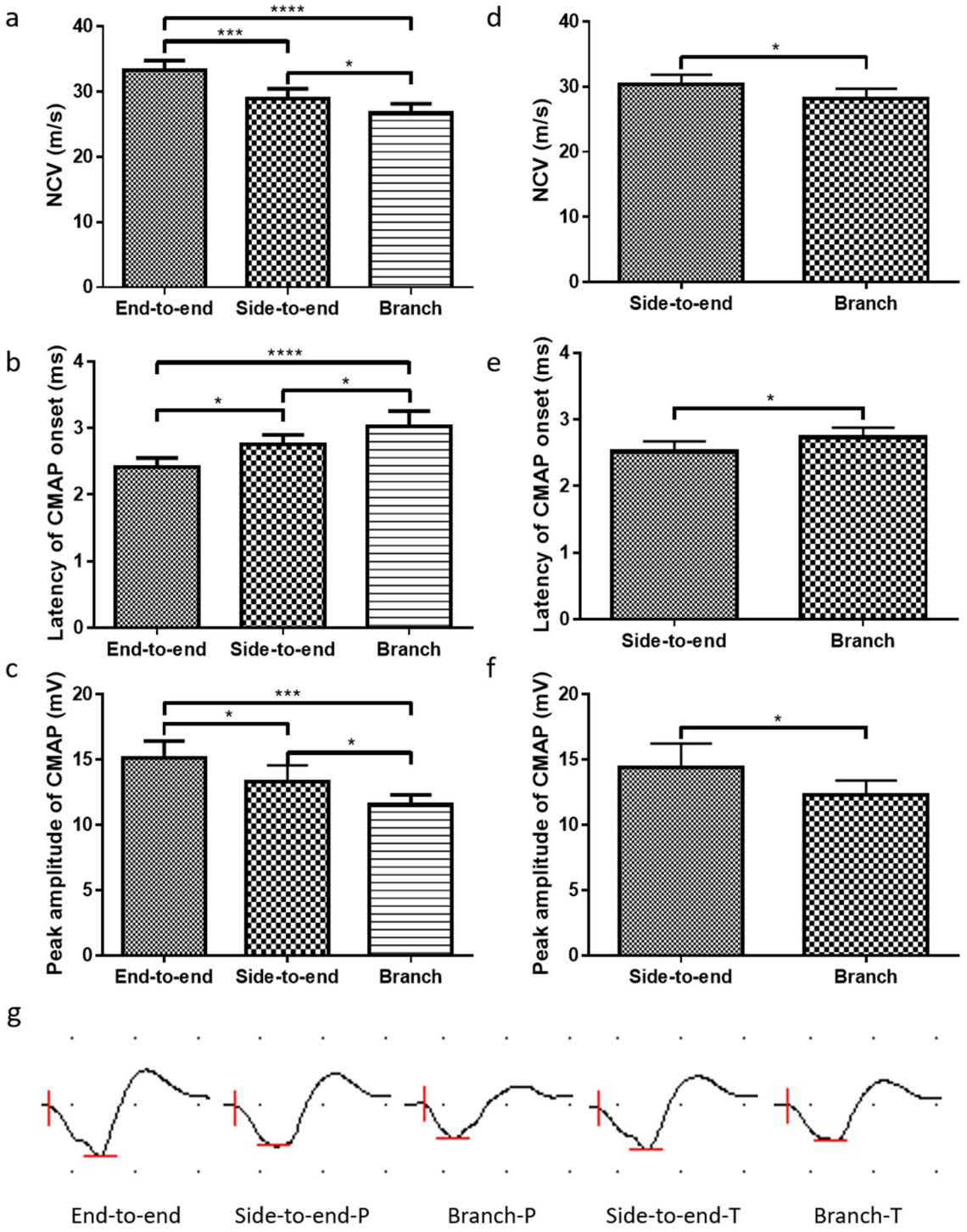

Figure 6. Efficacy of the 3D-printed two-branch nerve conduit *in vivo*. Electrophysiological parameters of the peroneal nerves: (**a**) nerve conduction velocity (NCV), (**b**) latency of compound muscle action potential (CMAP) onset and (**c**) peak amplitude of CMAP. Electrophysiological parameters of the tibial nerves: (**d**) NCV, (**e**) latency of CMAP onset and (**f**) peak amplitude of CMAP. (**g**) Representative waveforms of CMAP amplitude in each group (P: peroneal nerve, T: tibial nerve). Data are presented as the mean ± standard deviation, $^{*}p < 0.05$, $^{***}p < 0.001$, $^{****}p < 0.0001$

higher than that in the side-to-end group (28.9 m/s, $p < 0.001$) and branch group (26.7 m/s, $p < 0.0001$). The NCV in the side-to-end group was higher than that in the branch group ($p < 0.05$). Similar results were observed for the latency of CMAP onset and peak amplitude of CMAP. As shown in Figure 6b, the latency of CMAP onset in the end-to-end group (2.4 ms) was significantly shorter than that in the side-to-end group (2.8 ms, $p < 0.05$) and branch group (3.0 ms, $p < 0.0001$). The latency of CMAP onset in the side-to-end group was shorter than that in the branch group ($p < 0.05$).

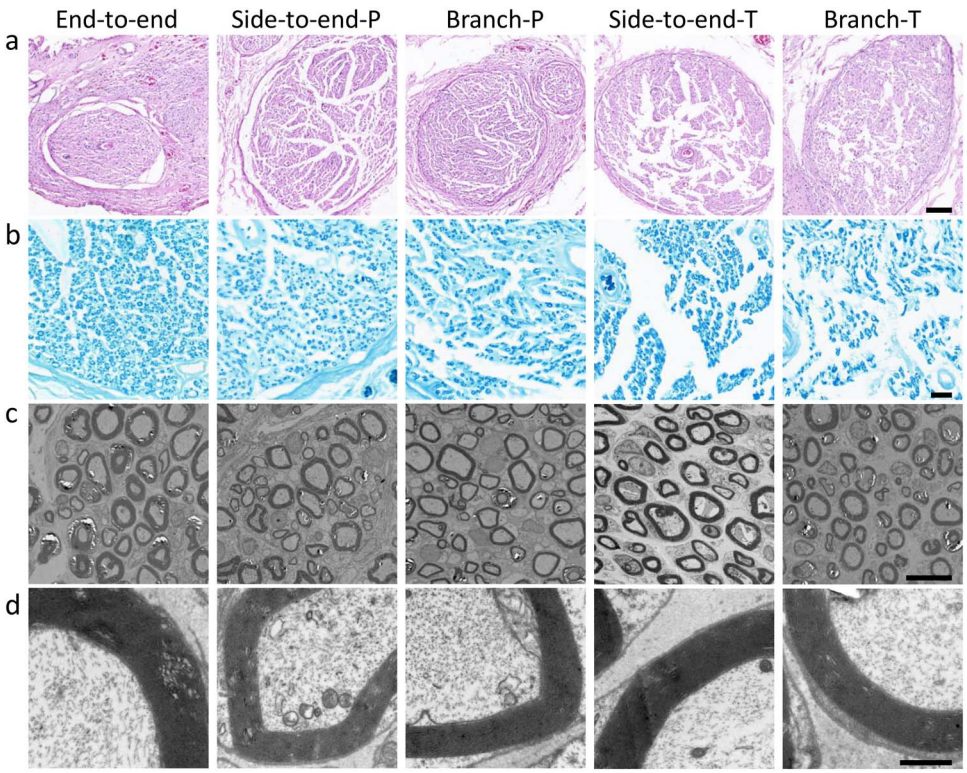

Figure 7. Histological evaluation of the regenerated nerves 3 months after surgery (P: peroneal nerve, T: tibial nerve). (**a**) Hematoxylin and eosin staining (scale bar = 100 μm) and (**b**) Luxol fast blue staining (scale bar = 20 μm) of the regenerated nerves. (**c**) Transmission electron microscopy images of regenerated axons and myelin sheaths (scale bar = 10 μm). (**d**) Magnification of (c) (scale bar = 1 μm)

As shown in Figure 6c, the peak amplitude of CMAP in the end-to-end group (15.1 mV) was significantly higher than that in the side-to-end group (13.3 mV, $p < 0.05$) and branch group (11.5 mV, $p < 0.001$). The peak amplitude of CMAP in the side-to-end group was higher than that in the branch group ($p < 0.05$). Electrophysiological examinations of the tibial nerves in the side-to-end group and branch group were also performed 3 months after surgery. As expected, the NCV in the side-to-end group (30.3 m/s) was higher than that in the branch group (28.2 m/s, $p < 0.05$) (Figure 6d). The latency of CMAP onset in the side-to-end group (2.5 ms) was shorter than that in the branch group (2.7 ms, $p < 0.05$) (Figure 6e). The peak amplitude of CMAP in the side-to-end group (14.4 mV) was higher than that in the branch group (12.3 mV, $p < 0.05$) (Figure 6f). The representative waveforms of CMAP amplitude in each group are shown in Figure 6g.

To further histologically evaluate nerve regeneration, the distal segments of the regenerated nerves were harvested and fixed immediately after electrophysiological analysis. As shown in Figure 7a, the images of H&E staining showed that the axons successfully regenerated along the conduits or autografts in all groups and were well organized. LFB staining was also performed to evaluate the myelination of regenerated axons. As shown in Figure 7b, the images of LFB staining showed that the axons were well myelinated along the axis of conduits or autografts. TEM observation was also performed to quantitatively evaluate the axon diameter and thickness of the myelin sheath (Figure 7c, d). As shown in Figure 8a, the axon diameter of the peroneal nerve in the end-to-end group (6.1 μm) was larger than that in the side-to-end group (4.9 μm, $p < 0.0001$) and branch group (4.6 μm, $p < 0.0001$). The axon diameter in the side-to-end group was larger than that in the branch group ($p < 0.05$). Similarly, the thickness of the myelin sheath of the peroneal nerve in the end-to-end group (1.14 μm) was thicker than that in the side-to-end group (0.92 μm, $p < 0.0001$) and branch group (0.86 μm, $p < 0.0001$) (Figure 8b). The thickness of the myelin sheath in the side-to-end group was thicker than that in the branch group ($p < 0.05$). Regarding the tibial nerve, the axon diameter in the side-to-end group (4.9 μm) was larger than that in the branch group (4.6 μm, $p < 0.05$) (Figure 8c). The thickness of the myelin sheath of the tibial nerve in the side-to-end group (0.95 μm) was thicker than that in the branch group (0.86 μm, $p < 0.05$) (Figure 8d).

After nerve injury, the targeted muscles will atrophy and be reinnervated once the axons regenerate and reach the muscles. The relative wet weight (surgical side to normal side) of the targeted muscles is an important value to evaluate reinnervation and functional restoration. The wet weights of the tibial anterior (innervated by the peroneal nerve) and gastrocnemius (innervated by the tibial nerve) were measured immediately after electrophysiological examinations. As shown in Figure 8e, the relative wet weight of the tibial anterior in

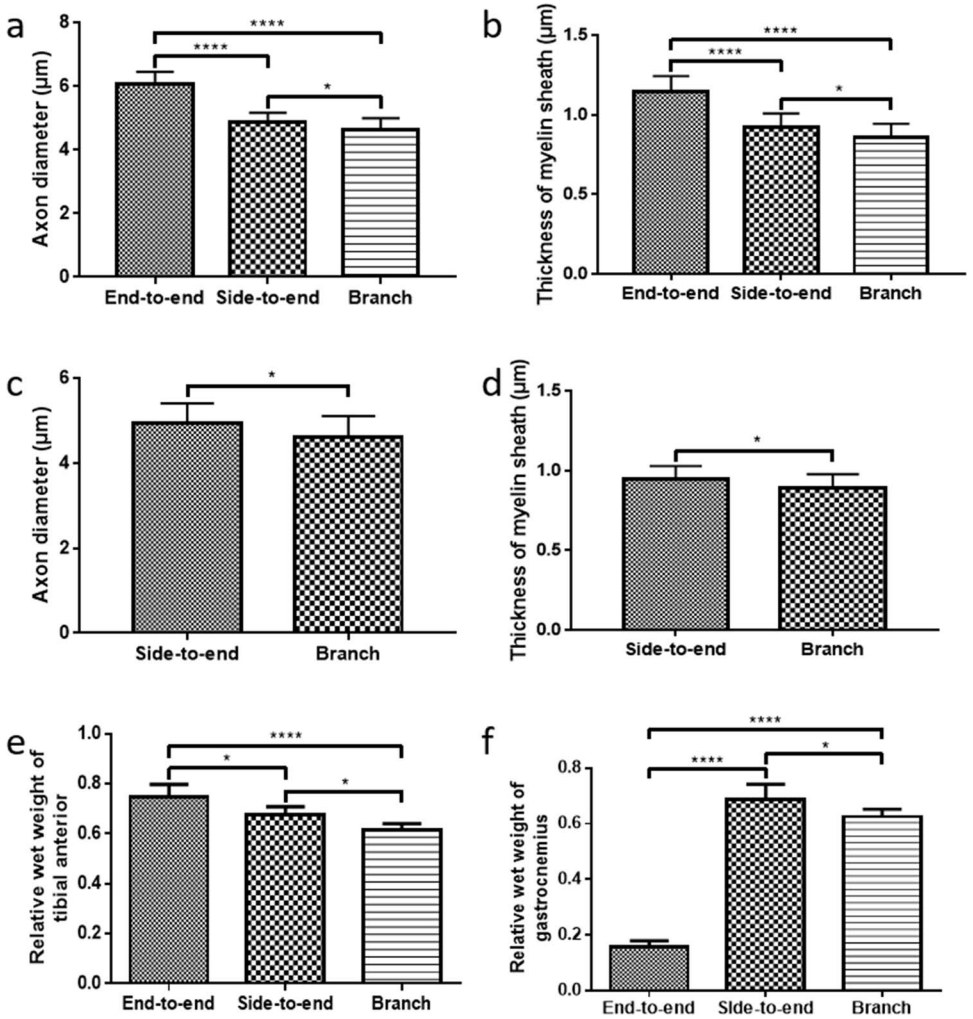

Figure 8. Quantitative analysis of (**a**) axon diameter and (**b**) and myelin sheath thickness of peroneal nerves. Quantitative analysis of (**c**) axon diameter and (**d**) myelin sheath thickness of tibial nerves. Relative wet weight of (**e**) tibial anterior and (**f**) gastrocnemius in each group. Data are presented as the mean ± standard deviation, $^{*}p < 0.05$, $^{****}p < 0.0001$

the end-to-end group (0.75) was significantly higher than that in the side-to-end group (0.67, $p < 0.05$) and branch group (0.61, $p < 0.0001$). The relative wet weight of the tibial anterior in the side-to-end group was higher than that in the branch group ($p < 0.05$). Since the distal tibial nerve in the end-to-end group was not preserved, the relative wet weight of the gastrocnemius in the end-to-end group (0.16) was much lower than that in the side-to-end group (0.69, $p < 0.0001$) and branch group (0.63, $p < 0.0001$) (Figure 8f). The relative wet weight of the gastrocnemius in the side-to-end group was higher than that in the branch group ($p < 0.05$).

Discussion

In this study, we found that a single nerve stump could form a complex nerve network in a 3D-printed multibranch conduit. Then, a 3D-printed two-branch nerve conduit was fabricated for nerve transfer. Among the three experimental groups, as expected, the peroneal nerve achieved the best functional recovery in the end-to-end group, because it was repaired by the whole tibial nerve. However, the complete transection of the tibial nerve resulted in its functional loss in the end-to-end group. In contrast, our branch conduit both repaired the injured peroneal nerve and preserved the function of the tibial nerve, suggesting its potential utility.

In the side-to-end group, the peroneal nerve and tibial nerve both achieved better functional recovery compared to the branch group. The reason might be that in the side-to-end group, the peroneal nerve was repaired by autograft and the tibial nerve was not completely transected, while in the branch group, they were both repaired by conduit. The nerve regeneration ability of a nonfunctional nerve conduit is usually inferior to that of an autograft. This is one limitation of our branch nerve conduit. However, an increasing number of studies have found that functional nerve conduits can promote nerve regeneration [22,23]. For instance, we previously found that cell-loaded or drug-loaded nerve conduits were

superior to nonfunctional nerve conduits and had regeneration ability comparable to that of autografts [15,16,24]. Thus, we could fabricate functional branch nerve conduits for better nerve regeneration in nerve transfer in the future.

3D printing has numerous applications and is a promising technology in tissue engineering and regenerative medicine [25]. In recent years, the use of 3D printing technology for promoting peripheral nerve regeneration has gained wide attention [2]. Uz *et al*. 3D-printed gelatine-based nerve conduits and demonstrated the importance of controlling the 3D microstructure to promote peripheral nerve regeneration [26]. Ouyang *et al*. found that uniaxially aligned seamless 3D-printed nerve guides could promote axon regeneration and myelination [27]. In nerve transfer, the most important role of 3D printing in branch conduits is customized manufacturing, allowing for tissue-matched conduit fabrication. Through precise 3D printing, multibranch nerve conduits could be fabricated and used to repair complicated nerve networks with a single nerve.

Another advantage of our branch nerve conduit is the use of artificial materials instead of autologous nerve grafts (autografts). Sometimes, the donor nerve and injured nerve are not close enough, and an interposition nerve graft is needed, for example in some cases of hypoglossal-facial nerve anastomosis [5,6], masseteric-facial nerve anastomosis [8], cross-face nerve grafting in facial nerve repair surgery [8] and nerve transfer in brachial plexus injuries [28,29]. The patient's own sural nerve is a commonly used autograft, but the autograft has several limitations, such as donor site morbidity, the possibility of neuroma formation and the need for additional surgery [1]. Due to the shortcomings of autografts, artificial nerve conduits have been increasingly investigated and considered as an alternative to autografts [2,30]. In this study, GelMA hydrogel, which has high hydrophilicity, was used to construct nerve conduits. Our results showed that GelMA hydrogels are suitable for 3D printing and have good biocompatibility both *in vitro* and *in vivo*. Apart from the characteristics of the nerve conduit in this study, our previous research also suggests that the nerve conduit has good permeability, which may promote the transportation of nutrients and blood supply [15]. In addition, the nerve conduit could eventually be degraded and no further operation is needed to remove the nerve conduit [15,16]. Previous studies also proved the potential utility of GelMA hydrogels in nerve repair [15,31–33] and muscle tissue engineering [34]. Meanwhile, researchers are trying to improve the efficacy of hydrogels by integrating GelMA with a conductive structure [35] or exploring better substitution hydrogels [36].

Previous studies have investigated the mechanism of nerve regeneration in bifurcated nerve conduits. Chiu *et al*. found that the distal nerve stump had a guiding influence towards the regeneration nerve fibers using branch conduits [37]. Abernethy *et al*. fabricated a double Y-shaped tube and the results obtained suggested that axons could regenerate along every bifurcation of the tube even without a distal nerve stump [38]. Muheremu *et al*. used Y-shaped conduits to repair nerve bifurcation defects and found it to be effective [39]. To our knowledge, we are the first to use branch nerve conduits in nerve transfer surgery and show good outcomes. In addition, researchers have demonstrated that direct nerve suturing could cause misdirection of newly grown axons, which may negatively affect functional recovery [39–41]. It has also been determined that Y-shaped nerve conduits can reduce collateral axonal branching [42,43]. Thus, apart from the above-mentioned advantages, our branch nerve conduit may also avoid axonal misdirection, which can enhance functional recovery of nerves.

Conclusions

In this study, we found that a single nerve stump could form a complex nerve network in a 3D-printed multibranch conduit. In nerve transfer, *in vivo* studies suggested that the 3D-printed two-branch nerve conduit could both repair the injured nerve and preserve partial function of the donor nerve, suggesting its potential clinical utility in nerve transfer.

Abbreviations

CCK-8: Cell Counting Kit-8; CMAP: Compound muscle action potential; DLP: Digital light processing; DMA: Dynamic mechanical analyzer; DMEM: Dulbecco's modified Eagle's medium; GelMA: Gelatine-methacryloyl; H&E: Hematoxylin and eosin; LAP: Lithium phenyl-2,4,6-trimethyl-benzoylphosphinate; LFB: Luxol fast blue; NCV: Nerve conduction velocity; SD: Sprague–Dawley; SEM: Scanning electron microscopy; TEM: Transmission electron microscopy.

Authors' contributions

JZ, JT and MG designed the experiments. JZ, JT, HC, HL, WW and YD carried out the experiments. JZ prepared the manuscript. JZ, JT, HL, WW, XL, MG, SY and JX revised the manuscript. SY and JX supervised the project. All authors contributed to discussion and analysis of the data. All authors read and approved the final manuscript.

Ethics approval and consent to participate

All animal experimental procedures were approved by the Institutional Animal Care and Use Committee of West China Hospital of Sichuan University and conformed to the guidelines and regulations of Sichuan University Committee on Animal Research and Ethics.

Conflict of interest

The authors declared no potential conflict of interest.

Data availability

The datasets used and/or analyzed during the current study are available from the corresponding authors on reasonable request.

Acknowledgments

The work was supported by Key Research and Development Projects of People's Liberation Army (BWS17J036), 1•3•5 project for disciplines of excellence, West China Hospital, Sichuan University (ZYJC18017, ZYJC18007), Cooperation Special Fund Project of Sichuan University-Panzhihua (2019CDPZH-17), Science and Technology Project of Chengdu (2018-CY02-00041-GX) and Sichuan Science and Technology Program (2021YFS0082). The authors would like to thank Dr Shuai Wang (West China Hospital, Sichuan University) for her help during the experiments.

References

1. Mokarram N, Dymanus K, Srinivasan A, Lyon JG, Tipton J, Chu J, *et al.* Immunoengineering nerve repair. *Proc Natl Acad Sci U S A*. 2017;114:E5077–e84.
2. Dixon AR, Jariwala SH, Bilis Z, Loverde JR, Pasquina PF, Alvarez LM. Bridging the gap in peripheral nerve repair with 3D printed and bioprinted conduits. *Biomaterials*. 2018;186:44–63.
3. Aszmann OC, Roche AD, Salminger S, Paternostro-Sluga T, Herceg M, Sturma A, *et al.* Bionic reconstruction to restore hand function after brachial plexus injury: a case series of three patients. *Lancet*. 2015;385:2183–9.
4. Quant EC, Jeste SS, Muni RH, Cape AV, Bhussar MK, Peleg AY. The benefits of steroids versus steroids plus antivirals for treatment of Bell's palsy: a meta-analysis. *BMJ*. 2009;339:b3354.
5. Manni JJ, Beurskens CH, van de Velde C, Stokroos RJ. Reanimation of the paralyzed face by indirect hypoglossal-facial nerve anastomosis. *Am J Surg*. 2001;182:268–73.
6. Le Clerc N, Herman P, Kania R, Tran H, Altabaa K, Tran Ba Huy P, *et al.* Comparison of 3 procedures for hypoglossal-facial anastomosis. *Otol Neurotol*. 2013;34:1483–8.
7. Vincent AG, Bevans SE, Robitschek JM, Wind GG, Hohman MH. Masseteric-to-facial nerve transfer and selective Neurectomy for rehabilitation of the Synkinetic smile. *JAMA Facial Plast Surg*. 2019;21:504–10.
8. Biglioli F, Frigerio A, Colombo V, Colletti G, Rabbiosi D, Mortini P, *et al.* Masseteric-facial nerve anastomosis for early facial reanimation. *J Craniomaxillofac Surg*. 2012;40:149–55.
9. Bertelli JA, Ghizoni MF. A surgical approach for concomitant spinal cord and brachial plexus surgery: an anatomical study. *Chir Main*. 1998;17:159–64.
10. Bertelli JA, Mira JC, Pecot-Dechavassine M, Sebille A. Selective motor hyperreinnervation using motor rootlet transfer: an experimental study in rat brachial plexus. *J Neurosurg*. 1997;87:79–84.
11. Zhu W, Ma X, Gou M, Mei D, Zhang K, Chen S. 3D printing of functional biomaterials for tissue engineering. *Curr Opin Biotechnol*. 2016;40:103–12.
12. Wang P, Sun Y, Shi X, Shen H, Ning H, Liu H. 3D printing of tissue engineering scaffolds: a focus on vascular regeneration. *Biodes Manuf*. 2021;4:344–78.
13. Mei Q, Rao J, Bei HP, Liu Y, Zhao X. 3D bioprinting photo-Crosslinkable hydrogels for bone and cartilage repair. *Int J Bioprint*. 2021;7:367.
14. Zhu W, Tringale KR, Woller SA, You S, Johnson S, Shen H, *et al.* Rapid continuous 3D printing of customizable peripheral nerve guidance conduits. *Mater Today (Kidlington)*. 2018;21:951–9.
15. Tao J, Zhang J, Du T, Xu X, Deng X, Chen S, *et al.* Rapid 3D printing of functional nanoparticle-enhanced conduits for effective nerve repair. *Acta Biomater*. 2019;90:49–59.
16. Xu X, Tao J, Wang S, Yang L, Zhang J, Zhang J, *et al.* 3D printing of nerve conduits with nanoparticle-encapsulated RGFP966. *Appl Mater Today*. 2019;16:247–56.
17. Fairbanks BD, Schwartz MP, Bowman CN, Anseth KS. Photoinitiated polymerization of PEG-diacrylate with lithium phenyl-2,4,6-trimethylbenzoylphosphinate: polymerization rate and cytocompatibility. *Biomaterials*. 2009;30:6702–7.
18. Shirahama H, Lee BH, Tan LP, Cho NJ. Precise tuning of facile one-pot Gelatin Methacryloyl (GelMA) synthesis. *Sci Rep*. 2016;6:31036.
19. Gou M, Qu X, Zhu W, Xiang M, Yang J, Zhang K, *et al.* Bio-inspired detoxification using 3D-printed hydrogel nanocomposites. *Nat Commun*. 2014;5:3774.
20. Li G, Zhao X, Zhao W, Zhang L, Wang C, Jiang M, *et al.* Porous chitosan scaffolds with surface micropatterning and inner porosity and their effects on Schwann cells. *Biomaterials*. 2014;35:8503–13.
21. Wang Y, Wang W, Wo Y, Gui T, Zhu H, Mo X, *et al.* Orientated guidance of peripheral nerve regeneration using conduits with a microtube Array sheet (MTAS). *ACS Appl Mater Interfaces*. 2015;7:8437–50.
22. Huang Y, Wu W, Liu H, Chen Y, Li B, Gou Z, *et al.* 3D printing of functional nerve guide conduits. *Burns Trauma*. 2021;9:tkab011. https://doi.org/10.1093/burnst/tkab011.
23. Zhuang H, Bu S, Hua L, Darabi MA, Cao X, Xing M. Gelatin-methacrylamide gel loaded with microspheres to deliver GDNF in bilayer collagen conduit promoting sciatic nerve growth. *Int J Nanomedicine*. 2016;11:1383–94.
24. Hu Y, Wu Y, Gou Z, Tao J, Zhang J, Liu Q, *et al.* 3D-engineering of Cellularized conduits for peripheral nerve regeneration. *Sci Rep*. 2016;6:32184.
25. Tack P, Victor J, Gemmel P, Annemans L. 3D-printing techniques in a medical setting: a systematic literature review. *Biomed Eng Online*. 2016;15:115.
26. Uz M, Buyukoz M, Sharma AD, Sakaguchi DS, Altinkaya SA, Mallapragada SK. Gelatin-based 3D conduits for transdifferentiation of mesenchymal stem cells into Schwann cell-like phenotypes. *Acta Biomater*. 2017;53:293–306.
27. Ouyang Y, Huang C, Zhu Y, Fan C, Ke Q. Fabrication of seamless electrospun collagen/PLGA conduits whose walls comprise highly longitudinal aligned nanofibers for nerve regeneration. *J Biomed Nanotechnol*. 2013;9:931–43.
28. Songcharoen P. Management of brachial plexus injury in adults. *Scand J Surg*. 2008;97:317–23.
29. Socolovsky M, Di Masi G, Battaglia D. Use of long autologous nerve grafts in brachial plexus reconstruction: factors that affect the outcome. *Acta Neurochir*. 2011;153:2231–40.
30. Sarker MD, Naghieh S, McInnes AD, Schreyer DJ, Chen X. Regeneration of peripheral nerves by nerve guidance conduits: influence of design, biopolymers, cells, growth factors, and physical stimuli. *Prog Neurobiol*. 2018;171:125–50.

31. Zhang H, Xu J, Saijilafu. The effects of GelMA hydrogel on nerve repair and regeneration in mice with spinal cord injury. *Ann Transl Med* 2021;9:1147.
32. Chen J, Huang D, Wang L, Hou J, Zhang H, Li Y, *et al.* 3D bioprinted multiscale composite scaffolds based on gelatin methacryloyl (GelMA)/chitosan microspheres as a modular bioink for enhancing 3D neurite outgrowth and elongation. *J Colloid Interface Sci*. 2020;574:162–73.
33. Lin YX, Li SH, Huang WC. Fabrication of soft tissue scaffold-mimicked microelectrode arrays using enzyme-mediated transfer printing. *Micromachines (Basel)*. 2021;12:1057.
34. Ngan CGY, Quigley A, Williams RJ, O'Connell CD, Blanchard R, Boyd-Moss M, *et al.* Matured Myofibers in bioprinted constructs with in vivo vascularization and innervation. *Gels*. 2021;7:171.
35. Heo DN, Lee SJ, Timsina R, Qiu X, Castro NJ, Zhang LG. Development of 3D printable conductive hydrogel with crystallized PEDOT:PSS for neural tissue engineering. *Mater Sci Eng C Mater Biol Appl*. 2019;99:582–90.
36. Zhao C, Wu Z, Chu H, Wang T, Qiu S, Zhou J, *et al.* Thiol-rich multifunctional macromolecular Crosslinker for Gelatin-Norbornene-based bioprinting. *Biomacromolecules*. 2021;22:2729–39.
37. Chiu DT, Smahel J, Chen L, Meyer V. Neurotropism revisited. *Neurol Res*. 2004;26:381–7.
38. Abernethy DA, Thomas PK, Rud A, King RH. Mutual attraction between emigrant cells from transected denervated nerve. *J Anat*. 1994;184:239–49.
39. Muheremu A, Sun JG, Wang XY, Zhang F, Ao Q, Peng J. Combined use of Y-tube conduits with human umbilical cord stem cells for repairing nerve bifurcation defects. *Neural Regen Res*. 2016;11:664–9.
40. Shapira Y, Tolmasov M, Nissan M, Reider E, Koren A, Biron T, *et al.* Comparison of results between chitosan hollow tube and autologous nerve graft in reconstruction of peripheral nerve defect: an experimental study. *Microsurgery*. 2016;36:664–71.
41. de Ruiter GC, Spinner RJ, Verhaagen J, Malessy MJ. Misdirection and guidance of regenerating axons after experimental nerve injury and repair. *J Neurosurg*. 2014;120:493–501.
42. Hizay A, Ozsoy U, Demirel BM, Ozsoy O, Angelova SK, Ankerne J, *et al.* Use of a Y-tube conduit after facial nerve injury reduces collateral axonal branching at the lesion site but neither reduces polyinnervation of motor endplates nor improves functional recovery. *Neurosurgery*. 2012;70:1544–56.
43. Ozsoy U, Demirel BM, Hizay A, Ozsoy O, Ankerne J, Angelova S, *et al.* Hypoglossal-facial anastomosis (HFA) over a 10 mm gap bridged by a Y-tube-conduit enhances neurite regrowth and reduces collateral axonal branching at the lesion site. *Restor Neurol Neurosci*. 2011;29:227–42.